



Published in final edited form as:

*Circulation*. 2018 June 05; 137(23): 2478–2493. doi:10.1161/CIRCULATIONAHA.117.033144.

## CD301b/MGL2<sup>+</sup> mononuclear phagocytes orchestrate autoimmune cardiac valve inflammation and fibrosis

Lee A Meier, BS, BBmE<sup>1,2,5</sup>, Jennifer L Auger, BA<sup>1,2</sup>, Brianna J Engelson, BA<sup>1,5</sup>, Hannah M Cowan<sup>1</sup>, Elise R Breed, BA<sup>3,5</sup>, Mayra I Gonzalez-Torres, BS<sup>1,2,5</sup>, Joshua D. Boyer, MS<sup>6</sup>, Mayank Verma, BS<sup>4,5</sup>, Aubyn Marath, MBBS, MS<sup>7</sup>, and Bryce A Binstadt, MD, PhD<sup>1,2,5</sup>

<sup>1</sup>Center for Immunology

<sup>2</sup>Department of Pediatrics

<sup>3</sup>Department of Laboratory Medicine and Pathology

<sup>4</sup>Department of Integrative Biology and Physiology

<sup>5</sup>University of Minnesota Medical School, Minneapolis, MN

<sup>6</sup>Department of Medicine, University of California, San Diego, CA

<sup>7</sup>CardioStart International, Tampa, FL

### Abstract

**BACKGROUND**—Valvular heart disease (VHD) is common and affects the mitral valve (MV) most frequently. Despite the prevalence of mitral valve disease (MVD), the cellular and molecular pathways that initiate and perpetuate it are not well understood.

**METHODS**—K/B.g7 T cell receptor (TCR) transgenic mice spontaneously develop systemic autoantibody-associated autoimmunity, leading to fully-penetrant fibro-inflammatory MVD and arthritis. We used multiparameter flow cytometry, intracellular cytokine staining, and immunofluorescent staining to characterize the cells in inflamed K/B.g7 MVs. We used genetic approaches to study the contribution of mononuclear phagocytes (MNP) to MVD in this model. Specifically, we generated K/B.g7 mice in which either CX3CR1 or CD301b/MGL2-expressing MNPs were ablated. Using K/B.g7 mice expressing *Cx3Cr1-Cre*, we conditionally deleted critical inflammatory molecules from MNPs, including the Fc receptor signal-transducing tyrosine kinase Syk and the cell adhesion molecule very late antigen-4 (VLA-4). We performed complementary studies using monoclonal antibodies to block key inflammatory molecules. We generated bone marrow chimeric mice to define the origin of the inflammatory cells present in the MV and to determine which valve cells respond to the pro-inflammatory cytokine TNF. Finally, we examined specimens from patients with rheumatic heart disease (RHD) to correlate our findings to human pathology.

---

Corresponding Author: Bryce A. Binstadt, Center for Immunology, University of Minnesota, Wallin Medical Biosciences Building, 2101 6<sup>th</sup> St. SE 2-114, Minneapolis, MN 55455, Telephone: 612-625-2953, Fax 612-625-2199, binstadt@umn.edu.  
Twitter handle (Lee A Meier): @LAMEier0158

### DISCLOSURES

LAM is an inventor on a pending patent related to the treatment of valvular heart disease (US20150164631 A1) currently under license to Vascudyne, Inc (Plano, TX). The contents of the submitted manuscript fall outside of this agreement.

**RESULTS**—MNPs comprised the vast majority of MV-infiltrating cells; these MNPs expressed CX3CR1 and CD301b/MGL2. Analogous cells were present in human RHD valves. K/B.g7 mice lacking CX3CR1 or in which CD301b/MGL2-expressing MNPs were ablated were protected from MVD. The valve-infiltrating CD301b/MGL2+ MNPs expressed tissue-reparative molecules including arginase-1 (Arg-1) and resistin-like molecule alpha (RELM- $\alpha$ ). These MNPs also expressed the pro-inflammatory cytokines TNF and IL-6, and antibody-blockade of these cytokines prevented MVD. Deleting Syk from CX3CR1-expressing MNPs reduced their TNF and IL-6 production and also prevented MVD. TNF acted through TNFR1 expressed on valve-resident cells to increase expression of vascular cell adhesion molecule-1 (VCAM-1). Conditionally deleting the VCAM-1 ligand VLA-4 from CX3CR1-expressing MNPs prevented MVD.

**CONCLUSIONS**—CD301b/MGL2+ MNPs are key drivers of autoimmune MVD in K/B.g7 mice and are also present in human RHD. We define key inflammatory molecules that drive MVD in this model, including Syk, TNF, IL-6, VLA-4, and VCAM-1.

### Keywords

valve; fibrosis; macrophage; inflammation; rheumatic heart disease; autoimmune

---

## INTRODUCTION

Valvular heart disease (VHD) is common and affects ~2.5% of all adults and ~14% of adults over the age of 75 in industrialized nations<sup>1</sup>. The mitral valve (MV) is most frequently diseased, followed by the aortic valve (AoV), while the right-sided valves (i.e. tricuspid valve [TV] and pulmonic valve [PV]) are only rarely affected<sup>1</sup>. In the setting of systemic autoimmune and inflammatory diseases such as rheumatic fever (RF) and systemic lupus erythematosus (SLE), MV pathology is common<sup>2</sup>. The molecular and cellular pathways that connect systemic inflammation to VHD have not been delineated.

Animal models have been used to study the link between systemic inflammatory diseases and cardiovascular (CV) disease (CVD), but are largely focused on accelerated atherosclerosis<sup>3</sup>. Because of this, the majority of preclinical studies investigating CV inflammation use mouse models with genetic disruptions of lipid clearance. When fed a high-fat or ‘Western’ diet, these mice reliably develop extreme and non-physiological hypercholesterolemia, subsequently driving atherogenesis<sup>4</sup>. Although AoV lesions can arise in these mice<sup>5</sup>, MV disease (MVD) has historically been challenging to model experimentally.

Rheumatic heart disease (RHD) that follows inadequately-treated Group A streptococci (GAS) infection in humans most commonly affects the MV<sup>6</sup>. During the progression of valvular RHD, mitral regurgitation (MR) progresses to mitral stenosis (MS)<sup>6</sup>, owing to the presence of longstanding fibrosis and MV remodeling induced by chronic inflammation. Immunization of rodents with cardiac myosin or GAS peptides can induce the production of anti-cardiac autoantibodies that provoke cardiac valve inflammation. These models have provided information about the cellular and molecular drivers of valve inflammation in the setting of a systemic autoantibody-associated disease<sup>7, 8</sup>, and have also lent support to the molecular mimicry hypothesis<sup>9, 10</sup>. However, these studies, along with similar studies of

valves from patients with rheumatic carditis, provide primarily descriptive insight<sup>6, 11, 12</sup>. Thus, the mechanisms by which RF progresses to RHD remain undefined, and therapeutic intervention is largely limited to prophylactic antibiotics and, eventually, surgery. Although early recognition and treatment of GAS infection has reduced the morbidity and mortality associated with RHD in developed countries, it remains a significant health challenge worldwide with an estimated mortality of more than 300,000 individuals annually<sup>12</sup>.

Autoantibody formation occurs not only in rheumatic carditis, but also in many other forms of acquired CVD, arising both as a comorbidity of systemic autoimmunity (e.g. Libman-Sacks endocarditis in SLE and the antiphospholipid antibody syndrome) and also in the general population<sup>13, 14</sup>. The antigens targeted by CVD-associated autoantibodies are diverse and include cardiac-specific and ubiquitously-expressed ones<sup>15, 16</sup>. Due to the well-studied connection between low-density lipoprotein (LDL) and atherogenesis, the majority of animal studies have focused on autoantibodies with reactivity to apolipoproteins, particularly LDL and products of its metabolism (e.g. oxidized LDL [oxLDL]). These studies, however, provide conflicting information: both disease-ameliorating and disease-exacerbating roles for such autoantibodies have been reported<sup>17, 18</sup>; whether these animal models correlate to human disease is also unclear<sup>19</sup>.

We have described a mouse model of cardiac valve disease occurring in the context of chronic autoantibody-mediated arthritis<sup>20</sup>. T cell receptor transgenic “K/B.g7” arthritic mice develop fully-penetrant, spontaneous-onset cardiac valve inflammation and fibrosis independently of disrupted lipid trafficking, dietary intervention, or experimentally-induced hyperlipidemia<sup>21</sup>. As in humans, the left-sided valves are affected in K/B.g7 mice; MVD is 100% penetrant while the AoV is affected less frequently<sup>20</sup>. Autoimmunity occurs spontaneously in K/B.g7 mice – no immunization is needed. Production of high-titer immunoglobulin G (IgG) autoantibodies reactive to a ubiquitously-expressed antigen is critical to the systemic inflammatory process in this model<sup>22</sup>. Using constitutive knockout mice, we have previously shown that IgG-binding Fc receptors (Fc $\gamma$ Rs) are necessary for the MV disease<sup>23</sup>. In related studies, we demonstrated that K/B.g7 MVD depends on MNPs; systemic MNP depletion using clodronate liposomes confers protection from MV inflammation and fibrosis<sup>23</sup>. In the present study, we dissect the molecular pathways by which specific mononuclear phagocyte (MNP) populations provoke fibro-inflammatory MV pathology.

## METHODS

The data, analytic methods, and study materials will be made available upon request to other researchers for purposes of reproducing the results.

### Animals

All animal experiments were conducted in accordance with the University of Minnesota Institutional Animal Care and Use Committee (IACUC) guidelines for the ethical care and treatment of laboratory animals (IACUC protocol #1506-32700A). The following mouse lines were provided by the indicated investigators: KRN T cell receptor (TCR) transgenic (‘KRN’) and C57BL/6:I-A<sup>g7</sup> MHC class II congenic (‘B.g7’), (D. Mathis, C. Benoist, and

the Institut de Génétique et Biologie Moléculaire et Cellulaire [IGBMC], Illkirch-Graffenstaden, France), *Itga4<sup>tm1Tpa</sup>* (*Itga4<sup>flb</sup>*, T. Papayannopoulou, University of Washington, Seattle). The remaining mice were purchased from The Jackson Laboratory: B6.129P2-*Syk<sup>tm1.2Tara</sup>*/J (*Syk<sup>flb</sup>*), B6J.B6N(Cg)-*Cx3cr1<sup>tm1.1(cre)Jung</sup>*/*Cx3cr1-Cre*), B6.129P-Cx3cr1<sup>tm1Litt</sup>/J (*Cx3cr1-gfp*), B6(FVB)-*Mgl2<sup>tm1.1</sup>*(HBEGF/EGFP)Aiwsk/J (*Mgl2-DTR*), B6.129S7-*Rag1<sup>tm1Mom</sup>*/J (*Rag1<sup>-/-</sup>*), C57BL/6-*Tnfrsf1a<sup>tm1Imx</sup>*/J (*Tnfr1<sup>-/-</sup>*), NOD/ShiLtJ ('NOD'), B6.SJL-Ptprc<sup>a</sup> Pepc<sup>b</sup>/BoyJ (CD45.1-congenic C57BL/6). Standard housing in a specific pathogen free (SPF) facility was employed in all studies.

### Monoclonal antibody (mAb) inhibition

All neutralizing monoclonal antibodies (mAbs) for *in vivo* use were purchased from BioXCell. Species-matched isotype control antibodies were purchased from Jackson ImmunoResearch. Antibody solutions were diluted with sterile 0.9% saline to a final concentration of 1 mg/mL. The dosing regimen consisted of twice-weekly intraperitoneal (IP) mAb injections (200 µg mAb in 200 µL 0.9% saline) for four weeks. The following clones were used: IL-6 (MP5-20F3), TNF (MP6-XT22), TNFR2 (TR75-54.7), VLA-4 (PS/2), VCAM-1 (M/K-2.7), IL-18 (YIGIF74-1G7), GM-CSF (MP1-22E9), CCL2 (2H5), IL-1β (B122).

### Tissue isolation and digestion

Following CO<sub>2</sub> euthanasia, mouse hearts were removed and placed in cold RPMI with L-glutamine (Gibco) and 3% FBS. MVs were then isolated with the aid of a dissection microscope. MVs were suspended in pre-warmed RPMI containing 3% FBS, 10 mM 2-[4-(2-hydroxyethyl)-piperazin-1-yl]-ethanesulfonic acid (HEPES), 500 U/mL collagenase-2 (Worthington Biochemical, LS004174), 20 U/mL DNase I (Worthington Biochemical, LS002006). Samples were incubated at 37°C using a water bath with periodic trituration for 1 hour total enzyme exposure. Enzyme activity was quenched using 10 mL cold RPMI containing 3% FBS, and the digested samples were centrifuged at 300g for 5 minutes at 4°C. Pellets were suspended in cold PBS containing 2% bovine serum albumin (BSA, Roche) and passed through a 70 µm filter. To lyse erythrocytes, 0.100 mL ammonium-chloride-potassium (ACK) lysis buffer was added to each valve sample, followed by incubation at room temperature for 3 minutes. The lysis was quenched by adding 1.5 mL of cold PBS containing 2% BSA. The remaining digested tissue samples were centrifuged at 300g for 5 minutes at 4°C and the supernatants were discarded. The remaining pellets were suspended in PBS containing 2% BSA and used for flow cytometry analyses. For secondary lymphoid organs (SLOs), the samples were macerated in ACK buffer, passed through a 70 µm cell strainer, incubated in for 3 minutes to lyse erythrocytes, then centrifuged at 300g for 5 minutes at 4°C. The remaining pellets were suspended in 2% BSA in PBS and counted using a hemocytometer. Axillary, brachial, cervical, inguinal, popliteal, para-aortic, and mesenteric lymph nodes, and spleen from each animal were pooled.

### Intracellular cytokine staining (ICS)

For analysis of TNF and IL-6 production *in vivo*, a bolus of 250 µg brefeldin A (eBioscience, 00-4506-51) in 200 µL saline was injected into the peritoneal cavity of each animal three hours prior to euthanasia. Lymphoid tissues and hearts were prepared as

described above. For ICS experiments, all sample buffers used prior to sample fixation contained 3 µg/mL brefeldin A. After staining surface antigens, samples were fixed and permeabilized as described above. Anti-TNF (clone MP6-XT22, BioLegend), and anti-IL-6 (clone MP5-20F3, BioLegend) antibodies were added at 1 µg/mL for 30 minutes at room temperature, protected from light. Each sample was subsequently washed three times using PBS containing 2% BSA, filtered through a 70 µm cell strainer, and used for flow cytometry analyses as described above.

### Flow cytometry

Antibodies with the following specificities were used (clones listed, purchased from BioLegend unless noted otherwise): CD3e (145-2C11 and 17A2), CD4 (RM4-5 and GK1.5), B220 (RA3-6B2), Ly6G (1A8), CD11b (M1/70), F4/80 (BM8), CX3CR1 (SA011F11), Ly6C (AL-21, BD), CD301b/MGL2 (URA-1), CD64 (X54-5/7.1), CD16.2 (9E9), CD49d (R1-2), Syk (5F5), CD49d (R1-2, eBioscience), CD16/32 (2.4G2). 2-5 million cells per lymphoid tissue sample were used in flow cytometry experiments. All cells liberated from collagenase-digested valve tissue were analyzed. Viability staining was conducted using Live/Dead Fixable Aqua (Fisher), Sytox Red (Fisher), and Ghost Violet-510 (Tonbo), according to each manufacturer's recommended protocol. Fc receptors were blocked using anti-CD16/32 (α-FcγRII/III, Tonbo) at 5 µg/mL. Sample fixation and permeabilization was utilized for intracellular protein detection according to the manufacturer's protocol (Cytofix/Cytoperm™, BD Biosciences). We used BD LSR Fortessa and BD LSR II cytometers equipped with FACSDiva software for data acquisition and FlowJo version 10 for data analyses. Quantification of fluorescence intensity was conducted by normalizing the geometric mean fluorescence intensities (gMFI) to their respective fluorescence-minus-one (FMO) controls. This ratio, averaged across experimental and biological replicates, is presented when indicated.

### Mouse tissue histology

Hearts were excised and flash-frozen using Optimal Cutting Temperature (OCT) medium over dry ice and isopentane slurry. Coronal sections were taken at 7 µm thickness with a cryostat (Leica CM3050 S) and stored at -80°C until used. Hematoxylin and eosin (H&E) staining was conducted according to standard methods. Masson's trichrome staining was conducted according to the manufacturer's recommendations (Abcam, ab150686). Cardiac valve thickness was measured as described previously<sup>20, 23, 24</sup> using cellSens image acquisition software (Olympus). For immunofluorescence (IF), sections were fixed in chilled acetone for 20 minutes. Nonspecific binding was blocked using PBS containing 5% normal donkey serum (NDS, Jackson ImmunoResearch), 0.1% Tween-20 (Sigma), 5 µg/mL anti-CD16/32 (2.4G2, Tonbo), and 5 µg/mL anti-CD64 (goat polyclonal, Santa Cruz). For indirect IF, primary antibodies (anti-VCAM-1, 429-MVCAM.A, BioLegend; anti-TNFR1, rabbit polyclonal, Bioss; anti-TNFR2, TR75-42.4; anti-RELM-α/FIZZ-1, rabbit polyclonal, Peprotech; anti-arginase-I, rabbit polyclonal, Invitrogen) were used at a concentration of 5 µg/mL and incubated overnight in a humidified staining box at 4°C in PBS containing 5% NDS and 0.1% Tween-20. Secondary antibodies matched to the species of the blocking serum (or streptavidin-conjugated fluorochromes when detecting biotin-conjugated primary antibodies) were purchased from Jackson ImmunoResearch and used at a 1:800 dilution in

PBS containing 2.5% NDS and 0.1% Tween-20. For direct IF, all fluorochrome-conjugated antibodies (anti-CD301b/MGL2, URA-1; anti-CD64, X54-5/7.1; anti-CD45.1, A20; CD45.2, 104) were applied overnight at 4°C in a humidified staining box using a concentration of 5 µg/mL in PBS containing 5% NDS and 0.1% Tween-20, protected from light. Hoechst 33342 (ThermoFisher) at 1 µg/mL in PBS was applied for 10 minutes to counterstain nuclei. Samples were mounted using anti-fade medium (ThermoFisher) and imaged using an Olympus BX51 or a Leica DM6000B. For biotinylated antibodies, in addition to the blocking method described above, endogenous biotin blocking was performed according to the manufacturer's protocol (Abcam, ab3387). Exposures were matched to negative staining in isotype controls when appropriate. The FIJI distribution of ImageJ (NIH) was used for image analysis<sup>25</sup>.

### **Ablation of *Mgl2*-expressing cells**

Transgenic mice containing a diphtheria toxin (DT) receptor (DTR) construct within the *Mgl2* gene<sup>26</sup> were crossed to the K/B.g7 background. Beginning at 4-weeks of age, intraperitoneal injections of 1µg DT (Sigma, D0564) in 100 µL PBS were given to each animal every other day and continued until 8 weeks of age. Histological assessment of MV inflammation and fibrosis was conducted as described above.

### **Statistics**

Graphpad (Prism) was used for all statistical analyses. Two-tailed Mann-Whitney, non-parametric tests were employed for comparisons between two groups. For comparisons involving three or more groups, one-way analysis of variance (ANOVA) with post-hoc Tukey's test for multiple comparisons was employed. Statistical significance was defined as  $p < 0.05$ , and indicated as \* $p < 0.05$ , \*\* $p < 0.01$ , & \*\*\* $p < 0.005$ . Sample sizes are listed in the Figures and/or Figure Legends.

### **Extended Methods**

Additional experimental methods can be found in the Supplemental Material included with this manuscript ( '*Human heart valve histology*', '*Tissue clearing and mitral valve whole-mount imaging*', '*Image Analysis*', '*Anti-GPI titers and arthritis scoring*', '*Bone marrow chimeras*' ).

## **RESULTS**

### **Fully-penetrant, fibro-inflammatory cardiac valve pathology in K/B.g7 mice**

The K/B.g7 mouse develops systemic inflammation resulting from expression of a transgenic T cell receptor (TCR) termed 'KRN' that has specificity for a self-peptide derived from glucose-6-phosphate isomerase (GPI). T cell activation occurs when antigen presenting cells (APCs) expressing the I-A<sup>g7</sup> major histocompatibility complex-II (MHC-II) present endogenous GPI peptides to KRN-expressing T lymphocytes. These T cells then provide help to B lymphocytes, leading to their activation and, ultimately, production of high-titer anti-GPI autoantibodies, primarily IgG1 (summarized in Figure 1A)<sup>27–29</sup>. While the inflammatory process in K/B.g7 mice occurs systemically, the primary disease manifestations are fully-penetrant fibro-inflammatory cardiac valve disease and erosive

polyarthritis<sup>20, 23, 24, 30</sup>. MV inflammation begins at 3 weeks of age; by 8 weeks, accumulation of inflammatory cells and interstitial thickening is obvious (Figure 1B). Masson's trichrome staining provides a qualitative demonstration of the fibrotic and inflammatory process present within the inflamed MVs of K/B.g7 mice (Figure 1C). Collagen deposition characteristically results from thickening of the lamina fibrosa, predominantly near the high-pressure left ventricle (LV) lumen (left side of both images in C). By 8 weeks, MVs of K/B.g7 mice are fibrotic and thickened approximately 2.5-fold relative to non-inflamed B.g7 controls (lacking the KRN transgene) and remain so chronically (Figure 1D). Valve hydroxyproline content, a measure of collagen deposition, is similarly elevated (Figure 1E). When isolated K/B.g7 MVs are enzymatically dissociated and analyzed by flow cytometry, MNPs (macrophages [CD45.2<sup>+</sup>CD3e<sup>-</sup> B220<sup>-</sup>Ly6G<sup>-</sup> CD11b<sup>+</sup>CD64/FcγRI<sup>+</sup>] and monocytes [CD45.2<sup>+</sup>CD3e<sup>-</sup> B220<sup>-</sup>Ly6G<sup>-</sup> CD11b<sup>+</sup>CD64/FcγRI<sup>-</sup>]) constitute the vast majority of the accumulated leukocytes (Figure 1F), an observation consistent with our prior studies demonstrating that systemic depletion of phagocytes using clodronate liposomes prevents K/B.g7 MV inflammation and fibrosis<sup>23</sup>.

To determine whether the MNPs arise from valve-resident precursors or are recruited from the circulation, we generated BM chimeric mice. BM cells from inflamed K/BxN mice (equivalent to K/B.g7) congenically expressing CD45.1 were transferred intravenously to sublethally-irradiated CD45.2<sup>+/+</sup>; *Rag1*<sup>-/-</sup> recipients (Supplemental Figure 1A). Following a 10-week reconstitution period, the relative abundance of CD45.1 and CD45.2 expression within the inflamed valves was quantified using analysis of IF images (Supplemental Methods and Supplemental Figure 1B–C). Approximately 70% of the inflammatory cells in the valve arise from radio-resistant, recipient-derived CD45.2<sup>+/+</sup> leukocytes whereas approximately 30% arise from the CD45.1<sup>+/+</sup> transferred BM cells. This is also true for the ratios among total CD64/FcγRI<sup>-</sup> and tissue-reparative CD301b/MGL2-expressing macrophages (Supplemental Figure 1D–F). Thus, valve-resident MNPs provide the dominant contribution to the accumulated inflammatory cells in K/B.g7 MVs while bone marrow-derived phagocytes are minor constituents.

### **Cx3cr1-expressing mononuclear phagocytes are required for K/B.g7 cardiac valve inflammation and fibrosis**

*Cx3cr1* encodes CX3CR1, the fractalkine (CX3CL1) receptor, and is expressed broadly within the MNP system<sup>31</sup>. We crossed *Cx3cr1-gfp* mice to the K/B.g7 background. These mice contain an eGFP reporter construct in the endogenous *Cx3cr1* locus (Figure 2A). Heterozygosity of the reporter allele (*Cx3cr1<sup>gfp/wt</sup>*) does not change MV fibrosis and thickening, and eGFP-positive cells are present diffusely within the MV interstitium (Figure 2B, top). *En face* imaging of *Cx3cr1<sup>gfp/wt</sup>*-K/B.g7 MVs that had undergone tissue-clearing reveals characteristic phagocyte morphology among the eGFP-positive cells infiltrating the mitral atrialis (Figure 2B, bottom). These CX3CR1-expressing cells bear morphological resemblance to a population of aortic and cardiac valve dendritic cells (DCs) described recently, and also to atrioventricular (AV) node macrophages that facilitate cardiac conduction<sup>32, 33</sup>. K/B.g7 mice homozygous for the *Cx3cr1-gfp* reporter allele lack endogenous CX3CR1 expression and are protected from MVD (Figure 2C). Flow cytometry of inflamed K/B.g7 mitral valves from *Cx3cr1<sup>gfp/wt</sup>* mice demonstrates that the CX3CR1-

expressing cells are nearly uniform in their expression of CD64/Fc $\gamma$ RI, the high-affinity IgG receptor commonly used to delineate a macrophage phenotype (Figure 2D). Taken together, these data demonstrate that CX3CR1-expressing MNPs are present in the inflamed MVs and are required for valve pathology.

### **CD301b/MGL2-expressing MNPs are required for K/B.g7 MV inflammation and fibrosis and have correlates in human inflammatory MV pathology**

The cell surface receptor CD301b/MGL2 is classically associated with type 2 inflammatory responses that dominate the reparative phase of wound-healing<sup>34</sup>. Immunofluorescent staining demonstrates that CD301b/MGL2<sup>+</sup> cells are distributed diffusely in inflamed K/B.g7 MVs and frequently co-localize with molecules associated with tissue repair and fibrosis including arginase-1 (Arg-1) and RELM- $\alpha$ /FIZZ-1 (Figure 3A, Supplemental Figure 2)<sup>26, 35, 36</sup>. To determine whether CD301b/MGL2-expressing MNPs are critical for MV inflammation, we generated *Mgl2-DTR* mice on the K/B.g7 background. These mice express the diphtheria toxin receptor (DTR) under control of the *Mgl2* promoter (Figure 3B, top); administration of DT ablates CD301b/MGL2-expressing cells. We find that DT-mediated ablation of CD301b/MGL2-expressing MNPs at the time of MVD onset (Figure 3B, right) significantly reduces MV fibro-inflammatory thickening (Figures 3C and D)

We next asked whether we could detect analogous cells expressing CD301/CLEC10A (the human ortholog to mouse CD301b/MGL2) in inflamed human MVs. Valve tissue samples were taken from patients with rheumatic carditis undergoing MV repair or replacement. Masson's trichrome staining demonstrates characteristic histopathology features of RF and RHD including perivascular inflammation and formation of granulomas (i.e. 'Aschoff bodies') (Supplemental Figure 3). These samples representing an early stage of RHD that presented clinically as MR display a disorganized and disrupted collagen fiber network with poorly staining regions of high proteoglycan (PG) and glycosaminoglycan (GAG) (Figure 3D, top). Immunostaining for human CD163 (pan-macrophage) and human CD301/CLEC10A demonstrates frequent co-localization of the markers (Figure 3D, bottom). Thus, like K/B.g7 MVD, human inflammatory MV pathology demonstrates accumulation of CD301-expressing macrophages.

### **TNF- and IL-6-producing CX3CR1<sup>+</sup>CD301b/MGL2<sup>+</sup> MNPs are enriched in inflamed K/B.g7 cardiac valves and promote valve inflammation and fibrosis**

We next sought to define the functional role for MNPs in K/B.g7 MV inflammation and fibrosis and hypothesized that they produce cytokines that drive MV inflammation. We tested this using intracellular cytokine staining (ICS) and flow cytometry of inflammatory cells isolated from K/B.g7 MVs. The CX3CR1-expressing MNPs can be subdivided based on Ly6C expression, with Ly6C-low and Ly6C-high cells thought to represent early- and late-stage recruited cells, respectively<sup>35, 37, 38</sup>. Both of these fractions contain pathogenic CD301b/MGL2<sup>+</sup> cells, and TNF and IL-6 production is readily detected in them (the gating strategy employed in identification of cytokine producing cells is shown in Figure 4A). Relative to pooled secondary lymphoid organs (axillary, brachial, cervical, inguinal, popliteal, para-aortic, mesenteric lymph nodes and spleen) of the same mice, the frequency of TNF- and IL-6-producing phagocytes isolated from inflamed MV tissue is significantly



elevated, demonstrating enrichment of cytokine-producing phagocytes within the inflamed MVs (Figure 4B). To determine the functional role for either cytokine in K/B.g7 MVD, we employed monoclonal antibody blockade of either TNF or IL-6 beginning at the onset of MV inflammation (Figure 4C). TNF or IL-6 neutralization resulted in qualitative and quantitative reductions in VCAM-1 intensity (Figures 4D and E). Compared to isotype control antibody-treated animals, blockade of either TNF or IL-6 significantly reduced MV fibrosis and thickening (Figure 4F). Additionally, no effect on MV thickening was observed using monoclonal antibody blockade of multiple other cytokines including IL-1 $\beta$  and CCL2 (Supplemental Figure 4, and *not shown*). Interestingly, blockade of either TNF or VCAM-1 beginning after the onset of MV inflammation (i.e. as interventions during established MVD) ameliorates MV fibrosis and thickening (Supplemental Figure 5), further underscoring the central role for TNF signaling and endothelial/stromal activation in K/B.g7 MVD. In sum, progression of K/B.g7 MVD exhibits a specific dependence on TNF and IL-6 stimulation. MV-infiltrating CX3CR1<sup>+</sup>CD301b<sup>+</sup> MNPs secrete TNF and IL-6 *in situ*, and neutralization of either cytokine prevents MV inflammation and fibrosis.

### Syk signaling in CX3CR1<sup>+</sup>CD301b/MGL2<sup>+</sup> phagocytes drives TNF and IL-6 production

We have previously demonstrated, using whole animal gene knockouts, that activation of immunoglobulin G (IgG) receptors (Fc $\gamma$ Rs, specifically Fc $\gamma$ RIII/CD32 and Fc $\gamma$ RIV/CD16.2) promotes MVD in K/B.g7 mice<sup>23</sup>. To determine if signaling downstream of activating Fc $\gamma$ Rs specifically in MNPs is necessary for K/B.g7 MVD, we employed a conditional gene deletion approach using *Cx3cr1-Cre*. Signal transduction downstream of activating Fc $\gamma$ Rs is mediated by an immunoreceptor tyrosine-based activation motif (ITAM)-bearing signaling chain that recruits spleen tyrosine kinase (Syk) (Figure 5A, left). To test whether this signaling pathway in MNPs is critical for MVD, we generated *Cx3cr1-Cre:Syk<sup>fl/fl</sup>* mice on the K/B.g7 background (Figure 5A, right). Mice lacking MNP expression of *Syk* (MNP-*Syk*) demonstrate significantly decreased MV inflammation and fibrotic thickening (Figure 5B). MNP-*Syk* promotes leukocyte accumulation in inflamed KB.g7 cardiac valves; total inflammatory cells (CD45.2<sup>+</sup>) are reduced by approximately 75% in the setting of conditional MNP-*Syk* deletion (Figure 5C). Similarly, the number of CD301b/MGL2-expressing MV cells is significantly reduced in mice lacking expression of MNP-*Syk* relative to *Cre*-negative littermates (Figure 5D). Intracellular cytokine staining and flow cytometry on MV inflammatory cells demonstrate that conditional MNP-*Syk*-deletion leads to a qualitative (Figure 5E) and quantitative (Figure 5F) reduction in TNF and IL-6 expression from valve-infiltrating CD301b/MGL2<sup>+</sup> MNPs. Thus, MNP-*Syk* is required for initiation and progression of MV inflammation and acts to promote TNF and IL-6 production from CD301b/MGL2<sup>+</sup> MNPs *in situ*.

### TNFR1 promotes MVD whereas TNFR2 restrains it

TNFR1 and TNFR2 have different cellular expression patterns and induce context-dependent effects<sup>39, 40</sup>. To clarify the mechanism of TNF-dependent MVD, we first evaluated expression TNF receptor-1 (TNFR1) and TNFR2 in inflamed MVs. Both receptors are readily detected in non-inflamed control (B.g7) and inflamed (K/B.g7) MVs (Figure 6A). We therefore interrogated the contribution of each of these receptors to the development and progression of MVD.

We hypothesized that valve-resistant cell types (e.g. endothelial cells [EC] and valvular interstitial cells [VIC]) expressing TNFR1 are the main responders to TNF. To test this, we generated BM chimeras with sub-lethally-irradiated *Tnfr1<sup>-/-</sup> Rag1<sup>-/-</sup>* mice reconstituted with *Tnfr1<sup>+</sup>* K/B.g7 BM. *Tnfr1<sup>+/+</sup> Rag1<sup>-/-</sup>* age-matched mice were used as control recipients (Figure 6B). MV fibrosis and thickening developed normally in the control animals, whereas recipient mice lacking *Tnfr1* expression on valve-resident cells failed to develop MVD (Figure 6C).

To assess the possible role of TNFR2, we used monoclonal antibody blockade according to timeline in Figure 6D. Interestingly, TNFR2 neutralization significantly exacerbated MV fibrosis and thickening compared to isotype control antibody-treated animals (Figure 6E), suggesting that TNFR2 normally inhibits MVD. Collectively, these studies demonstrate opposing roles for TNFR1 and TNFR2 — TNFR1 promotes MVD in K/B.g7 mice whereas TNFR2 restrains it.

### Accumulation of valve-infiltrating CX3CR1<sup>+</sup> MNPs depends on VCAM-1:VLA-4

Based on our studies demonstrating K/B.g7 MVD requires expression of TNF or IL-6, and that these cytokines promote VCAM-1 expression in inflamed MVs (Figure 4), we postulated that activation of the valve stroma following TNF or IL-6 stimulation leads to accumulation of CX3CR1<sup>+</sup> MNPs in a VCAM-1:VLA-4-dependent process (Figure 7A). We again used monoclonal antibody blockade, now targeting VCAM-1, VLA-4, or isotype control according to the timeline depicted in Figure 7B. Blockade of either VLA-4 or VCAM-1 significantly attenuated valve fibrosis and thickening (Figure 7B, top), both qualitatively (as demonstrated through H&E staining) and quantitatively, as demonstrated by MV thickness measurements in each case. We next sought to determine whether MNPs are the critical VLA-4-expressing population. Conditional deletion of alpha-4 integrin (*Itga4*, encoding the  $\alpha 4$  subunit of VLA-4) in MNPs using *Cx3cr1-Cre* (Figure 7C), prevents assembly and cell surface expression of the VLA-4 heterodimer ( $\alpha 4\beta 1$ ). Conditional deletion of *Itga4* in MNPs (MNP-*Itga4*) of K/B.g7 mice significantly reduces fibro-inflammatory MV thickening (Figure 7C). Flow cytometric analysis of valves from *Cx3cr1-Cre<sup>+/wt</sup>:Itga4<sup>fl/fl</sup>* mice (Figure 7D) demonstrates a significant quantitative reduction in accumulation of and CX3CR1<sup>+</sup>CD64/Fc $\gamma$ RI<sup>+</sup> MNPs (bearing a classical macrophage surface phenotype), relative to littermates lacking *Cre* expression. Thus, CX3CR1<sup>+</sup> MNPs accumulate in K/B.g7 MVs mice via expression of VLA-4 and through interactions with VCAM-1 expressed on the cytokine-activated valve stroma.

### Arthritis progression and autoantibody titers: MV-specific pathogenesis

The progression of arthritis and anti-GPI IgG titers were assessed in all of the experiments presented above (Supplemental Methods). In each setting, the interventions (e.g. monoclonal antibody blockade, conditional gene deletions, BM chimeras) had no effect on the progression of arthritis or anti-GPI IgG production (Supplemental Figures 6–9). Thus, K/B.g7 MVD progresses by distinct mechanisms from those contributing to joint pathology in the same animals. Additionally, the reductions in valve inflammation and fibrosis highlighted herein are not the result of global suppression of inflammation, as demonstrated by unimpeded development of arthritis and autoantibody production.

## DISCUSSION

Using complementary *in vivo* approaches including blocking antibodies, constitutive and conditional gene deletion, and targeted cell depletion, we define a critical inflammatory population of CD301b-expressing MNPs (also known as macrophage galactose N-acetyl-galactosamine specific lectin 2 [MGL2]) that is required for MV pathology and demonstrate that similar cells are present in MV specimens from human patients with rheumatic carditis. Our findings are consistent with the working model shown in Figure 8. Initial production of anti-GPI auto-antibodies results from the interaction of self-reactive T and B cells (1). Binding of circulating IgG auto-antibodies to activating IgG receptors (FcγRs) on valve-resident cardiac phagocytes (2), activates a Syk-dependent signaling cascade, resulting in TNF and IL-6 production (3). MNP-derived TNF acts through TNFR1 on the radio-resistant cell populations in the valve stroma and interstitium (4), upregulating VCAM-1. Circulating VLA-4<sup>+</sup> MNPs interact with VCAM-1 (5) and are recruited to the valve interstitium where they assume a tissue-reparative phenotype characterized by expression of CD301b/MGL2<sup>+</sup>(6)<sup>26, 34</sup>. To our knowledge, this is the first study to define the *in vivo* cellular and molecular mechanisms that mediate chronic autoimmune MV inflammation and fibrosis. More broadly, our findings advance the understanding of how circulating autoantibodies provoke cardiac pathology.

The immune system's contribution to CVD has been studied extensively<sup>41</sup>. It is well known that patients with systemic inflammatory disorders (e.g. rheumatoid arthritis, systemic lupus erythematosus) develop more accelerated and aggressive forms of CVD compared to the general population<sup>42</sup>. Independently of blood lipids, increased inflammatory biomarkers (e.g. C-reactive protein [CRP], IL-6) positively correlate with the risk of adverse CV events<sup>43</sup>. Despite these observations, no currently FDA-approved therapies directly target elements of adverse CV inflammation. In recent years much emphasis has been placed on understanding the mechanisms underlying immune-mediated CV remodeling. Medical management of CVD, however, has historically centered around blood lipids and, in particular, low-density lipoprotein (LDL) reduction; few large-scale clinical trials have directly evaluated the role of inflammation during the natural history of CVD.

The landmark CANTOS study provides direct confirmation for the role of inflammation in CV pathology. In this study, administration of an IL-1β neutralizing antibody (canakinumab) to patients with a prior history of myocardial infarction and evidence of elevated systemic inflammation (as indicated by elevated serum C-reactive protein) significantly reduced adverse CV events reference. IL-1β was chosen as a therapeutic target in view of its role in driving IL-6 production; serum levels of IL-6 demonstrate a strong, lipid-independent correlation with the risk of adverse CV events<sup>43-45</sup>. Herein, we demonstrate a critical role for both IL-6 and TNF as drivers of chronic cardiac valve inflammation in K/B.g7 mice, whereas IL-1β blockade had no effect. Thus, the pathways by which cardiac inflammation arise are diverse. The results of CANTOS confirm the role for inflammation in CVD and underscore the importance of continued exploration of additional pathways by which immune dysregulation may contribute to its development. While CANTOS provides much needed confirmation of the inflammation hypothesis in atherosclerotic CVD, additional immune mechanisms undoubtedly also contribute to CV pathology.

We have defined a critical role for CD301b/MGL2-expressing MNPs in a mouse model of systemic autoimmunity-associated MVD. Beyond its association with MNP (e.g. macrophage, DC) polarization during type 2 inflammatory responses in multiple disease models<sup>26, 34, 46</sup>, relatively little is known about the specific function(s) of CD301b/MGL2 and its human ortholog, CD301/CLEC10. Consistent with this, no prior studies have demonstrated that CD301b/MGL2 expression delineates a critical pathogenic MNP subset that is required for CV pathology. Most commonly, MGL2/CD301b is used in a descriptive manner to designate an alternatively-activated phenotype because of its association with canonical 'M2 macrophage' polarization. Studies have shown that white adipose provides a niche for CD301b/MGL2<sup>+</sup> MNPs. Therein, their functional roles are diverse and include regulation of whole-organism metabolic homeostasis through endocrine secretion of RELM $\alpha$ /FIZZ-1<sup>34</sup>. The well-defined connection between derangements of metabolism (e.g. diabetes, obesity) and cardiovascular risk tempts speculation about potential direct and indirect roles for adipose-residing CD301b/MGL2-expressing MNPs during CVD progression. Further study of the biology of CD301b/MGL2-expressing cells will be needed to clarify our experimental observations. In particular, determination of the specific anatomic compartments from which pathogenic CD301b/MGL2-expressing MNPs arise in K/B.g7 MVD as well as their temporal dynamics during MVD progression will both be greatly informative.

The most commonly-employed mouse models used to study lipid-mediated vascular remodeling and CVD are based on genetic disruption of lipid trafficking (i.e. *ApoE*<sup>-/-</sup> and *Ldlr*<sup>-/-</sup> mice on a high-fat diet). These models are characterized by extreme, non-physiological hyperlipidemia; how well they model human CVD is unclear, and the potential therapies that have emerged from these animal models failed to demonstrate efficacy in human clinical trials. Models that provide insight into other mechanisms underlying CVD pathology are therefore needed. Although K/B.g7 mice do develop mild spontaneous dyslipidemia on a normal chow diet<sup>21</sup>, they do not develop extreme hyperlipidemia. This model thus serves as a powerful tool to focus on the immune drivers of CV inflammation. FDA-approved therapies exist or are in development to target the pro-inflammatory mediators of CVD we have defined here, including TNF, IL-6, VLA-4, VCAM-1 and Syk<sup>47, 48</sup>. Thus, our study provides the basis for the rational design of clinical trials of agents such as these for patients with chronic inflammatory CVD.

## Supplementary Material

Refer to Web version on PubMed Central for supplementary material.

## Acknowledgments

The authors would like to acknowledge the following: University of Minnesota Cancer Center Flow Cytometry Resource (UFRCR, Paul Champoux, Jason Motl, and Terri Martin), Thalia Papayannopoulou, MD, DSci, (*Itga4*-floxed transgenic mice), and Christophe Benoist, Diane Mathis, and the Institute of Genetics and Molecular and Cellular Biology (IGBMC) (KRN transgenic, I-A<sup>g7</sup> congenic mice), Jop van Berlo, MD, PhD (critical manuscript review), Ms. Janine Henson, RN, BSN, CCRN, and surgical colleagues with CardioStart International, for coordinating international sample collections.

## SOURCES OF FUNDING

The following funding sources supported this work: NIH (R01-HL121093, T32-AI007313, T32-GM008244, R25-HL088728), Rheumatology Research Foundation (Innovative Research Grant, Medical and Graduate Student Preceptorship), Dr. Warren and Henrietta Warwick MD/PhD Fellowship. Research reported in this publication was supported by the National Center for Advancing Translational Sciences of the NIH Award Number UL1TR000114. The content is solely the responsibility of the authors and does not necessarily represent the official views of the NIH.

## References

1. Iung B, Vahanian A. Epidemiology of acquired valvular heart disease. *Can J Cardiol.* 2014; 30:962–970. DOI: 10.1016/j.cjca.2014.03.022 [PubMed: 24986049]
2. Levine RA, Hagege AA, Judge DP, Padala M, Dal-Bianco JP, Aikawa E, Beaudoin J, Bischoff J, Bouattia-Naji N, Bruneval P, Butcher JT, Carpentier A, Chaput M, Chester AH, Clusel C, Delling FN, Dietz HC, Dina C, Durst R, Fernandez-Friera L, Handschumacher MD, Jensen MO, Jeunemaitre XP, Le Marec H, Le Tourneau T, Markwald RR, Merot J, Messas E, Milan DP, Neri T, Norris RA, Peal D, Perrocheau M, Probst V, Puceat M, Rosenthal N, Solis J, Schott JJ, Schwammenthal E, Slangenaupt SA, Song JK, Yacoub MH. Mitral valve disease--morphology and mechanisms. *Nat Rev Cardiol.* 2015; 12:689–710. DOI: 10.1038/nrcardio.2015.161 [PubMed: 26483167]
3. Willerson JT, Ridker PM. Inflammation as a cardiovascular risk factor. *Circulation.* 2004; 109:ii2–10. DOI: 10.1161/01.cir.0000129535.04194.38 [PubMed: 15173056]
4. Nakashima Y, Plump AS, Raines EW, Breslow JL, Ross R. ApoE-deficient mice develop lesions of all phases of atherosclerosis throughout the arterial tree. *Arterioscler Thromb.* 1994; 14:133–140. [PubMed: 8274468]
5. Sider KL, Blaser MC, Simmons CA. Animal models of calcific aortic valve disease. *Int J Inflamm.* 2011; 2011:364310.doi: 10.4061/2011/364310 [PubMed: 21826258]
6. Marijon E, Mirabel M, Celermajer DS, Jouven X. Rheumatic heart disease. *Lancet.* 2012; 379:953–964. DOI: 10.1016/s0140-6736(11)61171-9 [PubMed: 22405798]
7. Rush CM, Govan BL, Sikder S, Williams NL, Ketheesan N. Animal models to investigate the pathogenesis of rheumatic heart disease. *Frontiers in pediatrics.* 2014; 2:116.doi: 10.3389/fped.2014.00116 [PubMed: 25414841]
8. Gorton D, Govan B, Olive C, Ketheesan N. B- and T-cell responses in group a streptococcus M-protein- or Peptide-induced experimental carditis. *Infect Immun.* 2009; 77:2177–2183. DOI: 10.1128/iai.01514-08 [PubMed: 19273562]
9. Li Y, Heuser JS, Cunningham LC, Kosanke SD, Cunningham MW. Mimicry and antibody-mediated cell signaling in autoimmune myocarditis. *J Immunol.* 2006; 177:8234–8240. [PubMed: 17114501]
10. Myers JM, Fairweather D, Huber SA, Cunningham MW. Autoimmune myocarditis, valvulitis, and cardiomyopathy. *Curr Protoc Immunol.* 2013; Chapter 15(Unit 15.14.11–51)doi: 10.1002/0471142735.im1514s101
11. Galvin JE, Hemric ME, Ward K, Cunningham MW. Cytotoxic mAb from rheumatic carditis recognizes heart valves and laminin. *J Clin Invest.* 2000; 106:217–224. [PubMed: 10903337]
12. Watkins DA, Johnson CO, Colquhoun SM, Karthikeyan G, Beaton A, Bukhman G, Forouzanfar MH, Longenecker CT, Mayosi BM, Mensah GA, Nascimento BR, Ribeiro ALP, Sable CA, Steer AC, Naghavi M, Mokdad AH, Murray CJL, Vos T, Carapetis JR, Roth GA. Global, Regional, and National Burden of Rheumatic Heart Disease, 1990–2015. *N Engl J Med.* 2017; 377:713–722. DOI: 10.1056/NEJMoa1603693 [PubMed: 28834488]
13. Caforio AL, Mahon NJ, Tona F, McKenna WJ. Circulating cardiac autoantibodies in dilated cardiomyopathy and myocarditis: pathogenetic and clinical significance. *Eur J Heart Fail.* 2002; 4:411–417. [PubMed: 12167378]
14. Chistiakov DA, Orekhov AN, Bobryshev YV. ApoA1 and ApoA1-specific self-antibodies in cardiovascular disease. *Lab Invest.* 2016; 96:708–718. DOI: 10.1038/labinvest.2016.56 [PubMed: 27183204]
15. Alard, J-E., Pers, J-O., Youinou, P., Jamin, C. Chapter 41 - Heat Shock Protein Autoantibodies. In: Gershwin, YSLME., editor. *Autoantibodies.* 3. San Diego: Elsevier; 2014. p. 343-348.

16. Rinaldi, M., Perricone, R., Perricone, C., Shoenfeld, Y. Chapter 42 - Antimyocardial Autoantibodies (AMCA). In: Gershwin, YSLME., editor. Autoantibodies. 3. San Diego: Elsevier; 2014. p. 349-355.
17. Hulthe J. Antibodies to oxidized LDL in atherosclerosis development--clinical and animal studies. *Clin Chim Acta*. 2004; 348:1–8. DOI: 10.1016/j.cccn.2004.05.021 [PubMed: 15369729]
18. Tsiantoulas D, Diehl CJ, Witztum JL, Binder CJ. B cells and humoral immunity in atherosclerosis. *Circ Res*. 2014; 114:1743–1756. DOI: 10.1161/circresaha.113.301145 [PubMed: 24855199]
19. Zhang J, Wang D, He S. Roles of antibody against oxygenized low density lipoprotein in atherosclerosis: recent advances. *Int J Clin Exp Med*. 2015; 8:11922–11929. [PubMed: 26550105]
20. Binstadt BA, Hebert JL, Ortiz-Lopez A, Bronson R, Benoist C, Mathis D. The same systemic autoimmune disease provokes arthritis and endocarditis via distinct mechanisms. *Proc Natl Acad Sci U S A*. 2009; 106:16758–16763. DOI: 10.1073/pnas.0909132106 [PubMed: 19805369]
21. Rose S, Eren M, Murphy S, Zhang H, Thaxton CS, Chowanec J, Waters EA, Meade TJ, Vaughan DE, Perlman H. A novel mouse model that develops spontaneous arthritis and is predisposed towards atherosclerosis. *Ann Rheum Dis*. 2013; 72:89–95. DOI: 10.1136/annrheumdis-2012-201431 [PubMed: 22736097]
22. Korganow AS, Ji H, Mangialaio S, Duchatelle V, Pelanda R, Martin T, Degott C, Kikutani H, Rajewsky K, Pasquali JL, Benoist C, Mathis D. From systemic T cell self-reactivity to organ-specific autoimmune disease via immunoglobulins. *Immunity*. 1999; 10:451–461. [PubMed: 10229188]
23. Hobday PM, Auger JL, Schuneman GR, Haasken S, Verbeek JS, Binstadt BA. Fcγ receptor III and Fcγ receptor IV on macrophages drive autoimmune valvular carditis in mice. *Arthritis & rheumatology (Hoboken, NJ)*. 2014; 66:852–862. DOI: 10.1002/art.38311
24. Haasken S, Auger JL, Binstadt BA. Absence of beta2 integrins impairs regulatory T cells and exacerbates CD4+ T cell-dependent autoimmune carditis. *J Immunol*. 2011; 187:2702–2710. DOI: 10.4049/jimmunol.1000967 [PubMed: 21795599]
25. Schindelin J, Arganda-Carreras I, Frise E, Kaynig V, Longair M, Pietzsch T, Preibisch S, Rueden C, Saalfeld S, Schmid B, Tinevez JY, White DJ, Hartenstein V, Eliceiri K, Tomancak P, Cardona A. Fiji: an open-source platform for biological-image analysis. *Nat Methods*. 2012; 9:676–682. DOI: 10.1038/nmeth.2019 [PubMed: 22743772]
26. Kumamoto Y, Linehan M, Weinstein JS, Laidlaw BJ, Craft JE, Iwasaki A. CD301b(+) dermal dendritic cells drive T helper 2 cell-mediated immunity. *Immunity*. 2013; 39:733–743. DOI: 10.1016/j.immuni.2013.08.029 [PubMed: 24076051]
27. Monach P, Hattori K, Huang H, Hyatt E, Morse J, Nguyen L, Ortiz-Lopez A, Wu HJ, Mathis D, Benoist C. The K/BxN mouse model of inflammatory arthritis: theory and practice. *Methods Mol Med*. 2007; 136:269–282. [PubMed: 17983155]
28. Monach PA, Benoist C, Mathis D. The role of antibodies in mouse models of rheumatoid arthritis, and relevance to human disease. *Adv Immunol*. 2004; 82:217–248. DOI: 10.1016/S0065-2776(04)82005-4 [PubMed: 14975258]
29. Matsumoto I, Maccioni M, Lee DM, Maurice M, Simmons B, Brenner M, Mathis D, Benoist C. How antibodies to a ubiquitous cytoplasmic enzyme may provoke joint-specific autoimmune disease. *Nat Immunol*. 2002; 3:360–365. DOI: 10.1038/ni772 [PubMed: 11896391]
30. Kouskoff V, Korganow AS, Duchatelle V, Degott C, Benoist C, Mathis D. Organ-specific disease provoked by systemic autoimmunity. *Cell*. 1996; 87:811–822. [PubMed: 8945509]
31. Jung S, Aliberti J, Graemmel P, Sunshine MJ, Kreutzberg GW, Sher A, Littman DR. Analysis of fractalkine receptor CX(3)CR1 function by targeted deletion and green fluorescent protein reporter gene insertion. *Mol Cell Biol*. 2000; 20:4106–4114. [PubMed: 10805752]
32. Hulsmans M, Clauss S, Xiao L, Aguirre AD, King KR, Hanley A, Hucker WJ, Wulfers EM, Seemann G, Courties G, Iwamoto Y, Sun Y, Savol AJ, Sager HB, Lavine KJ, Fishbein GA, Capen DE, Da Silva N, Miquerol L, Wakimoto H, Seidman CE, Seidman JG, Sadreyev RI, Naxerova K, Mitchell RN, Brown D, Libby P, Weissleder R, Swirski FK, Kohl P, Vinegoni C, Milan DJ, Ellinor PT, Nahrendorf M. Macrophages Facilitate Electrical Conduction in the Heart. *Cell*. 2017; 169:510–522. e520. DOI: 10.1016/j.cell.2017.03.050 [PubMed: 28431249]

33. Choi JH, Do Y, Cheong C, Koh H, Boscardin SB, Oh YS, Bozzacco L, Trumpfheller C, Park CG, Steinman RM. Identification of antigen-presenting dendritic cells in mouse aorta and cardiac valves. *J Exp Med*. 2009; 206:497–505. DOI: 10.1084/jem.20082129 [PubMed: 19221394]
34. Kumamoto Y, Camporez JPG, Jurczak MJ, Shanabrough M, Horvath T, Shulman GI, Iwasaki A. CD301b(+) Mononuclear Phagocytes Maintain Positive Energy Balance through Secretion of Resistin-like Molecule Alpha. *Immunity*. 2016; 45:583–596. DOI: 10.1016/j.immuni.2016.08.002 [PubMed: 27566941]
35. Varol C, Mildner A, Jung S. Macrophages: development and tissue specialization. *Annu Rev Immunol*. 2015; 33:643–675. DOI: 10.1146/annurev-immunol-032414-112220 [PubMed: 25861979]
36. Knipper JA, Willenborg S, Brinckmann J, Bloch W, Maass T, Wagener R, Krieg T, Sutherland T, Munitz A, Rothenberg ME, Niehoff A, Richardson R, Hammerschmidt M, Allen JE, Eming SA. Interleukin-4 Receptor alpha Signaling in Myeloid Cells Controls Collagen Fibril Assembly in Skin Repair. *Immunity*. 2015; 43:803–816. DOI: 10.1016/j.immuni.2015.09.005 [PubMed: 26474656]
37. Yona S, Kim KW, Wolf Y, Mildner A, Varol D, Breker M, Strauss-Ayali D, Viukov S, Williams M, Misharin A, Hume DA, Perlman H, Malissen B, Zelzer E, Jung S. Fate mapping reveals origins and dynamics of monocytes and tissue macrophages under homeostasis. *Immunity*. 2013; 38:79–91. DOI: 10.1016/j.immuni.2012.12.001 [PubMed: 23273845]
38. Molawi K, Wolf Y, Kandalla PK, Favret J, Hagemeyer N, Frenzel K, Pinto AR, Klapproth K, Henri S, Malissen B, Rodewald HR, Rosenthal NA, Bajenoff M, Prinz M, Jung S, Sieweke MH. Progressive replacement of embryo-derived cardiac macrophages with age. *J Exp Med*. 2014; 211:2151–2158. DOI: 10.1084/jem.20140639 [PubMed: 25245760]
39. Al-Lamki RS, Wang J, Vandenabeele P, Bradley JA, Thiru S, Luo D, Min W, Pober JS, Bradley JR. TNFR1- and TNFR2-mediated signaling pathways in human kidney are cell type-specific and differentially contribute to renal injury. *FASEB J*. 2005; 19:1637–1645. DOI: 10.1096/fj.05-3841com [PubMed: 16195372]
40. Venkatesh D, Hernandez T, Rosetti F, Batal I, Cullere X, Luscinskas FW, Zhang Y, Stavrakis G, Garcia-Cardena G, Horwitz BH, Mayadas TN. Endothelial TNF receptor 2 induces IRF1 transcription factor-dependent interferon-beta autocrine signaling to promote monocyte recruitment. *Immunity*. 2013; 38:1025–1037. DOI: 10.1016/j.immuni.2013.01.012 [PubMed: 23623383]
41. Libby P. Inflammation in atherosclerosis. *Arterioscler Thromb Vasc Biol*. 2012; 32:2045–2051. DOI: 10.1161/ATVBAHA.108.179705 [PubMed: 22895665]
42. Prasad M, Hermann J, Gabriel SE, Weyand CM, Mulvagh S, Mankad R, Oh JK, Matteson EL, Lerman A. Cardiorheumatology: cardiac involvement in systemic rheumatic disease. *Nat Rev Cardiol*. 2015; 12:168–176. DOI: 10.1038/nrcardio.2014.206 [PubMed: 25533796]
43. Ridker PM, Hennekens CH, Buring JE, Rifai N. C-reactive protein and other markers of inflammation in the prediction of cardiovascular disease in women. *N Engl J Med*. 2000; 342:836–843. DOI: 10.1056/NEJM200003233421202 [PubMed: 10733371]
44. Ridker PM, Danielson E, Fonseca FA, Genest J, Gotto AM Jr, Kastelein JJ, Koenig W, Libby P, Lorenzatti AJ, MacFadyen JG, Nordestgaard BG, Shepherd J, Willerson JT, Glynn RJ. Rosuvastatin to prevent vascular events in men and women with elevated C-reactive protein. *N Engl J Med*. 2008; 359:2195–2207. DOI: 10.1056/NEJMoa0807646 [PubMed: 18997196]
45. Ridker PM, Everett BM, Thuren T, MacFadyen JG, Chang WH, Ballantyne C, Fonseca F, Nicolau J, Koenig W, Anker SD, Kastelein JJP, Cornel JH, Pais P, Pella D, Genest J, Cifkova R, Lorenzatti A, Forster T, Kobalava Z, Vida-Simiti L, Flather M, Shimokawa H, Ogawa H, Dellborg M, Rossi PRF, Troquay RPT, Libby P, Glynn RJ, Group CT. Antiinflammatory Therapy with Canakinumab for Atherosclerotic Disease. *N Engl J Med*. 2017; doi: 10.1056/NEJMoa1707914
46. van Kooyk Y, Ilarregui JM, van Vliet SJ. Novel insights into the immunomodulatory role of the dendritic cell and macrophage-expressed C-type lectin MGL. *Immunobiology*. 2015; 220:185–192. DOI: 10.1016/j.imbio.2014.10.002 [PubMed: 25454488]
47. Liu D, Mamorska-Dyga A. Syk inhibitors in clinical development for hematological malignancies. *J Hematol Oncol*. 2017; 10:145. doi: 10.1186/s13045-017-0512-1 [PubMed: 28754125]

48. Singh S, Kumar N, Dwiwedi P, Charan J, Kaur R, Sidhu P, Chugh VK. Monoclonal Antibodies: A Review. *Curr Clin Pharmacol*. 2017; doi: 10.2174/1574884712666170809124728

Author Manuscript

Author Manuscript

Author Manuscript

Author Manuscript



## CLINICAL PERSPECTIVE

### What is new?

- We identify a critical population of CD301b/MGL2-expressing mononuclear phagocytes (MNPs) that orchestrates MV inflammation and fibrosis in a mouse model.
- We demonstrate an analogous cell population is present in human inflammatory cardiac valve disease.

### What are the clinical implications?

- To our knowledge, these are the first studies to define the cellular and molecular mechanisms of cardiac valve inflammation and fibrosis occurring in the setting of systemic inflammatory disease, such as that seen in rheumatic heart disease.
- We identify multiple potential therapeutic targets that are required for MV inflammation and fibrosis.

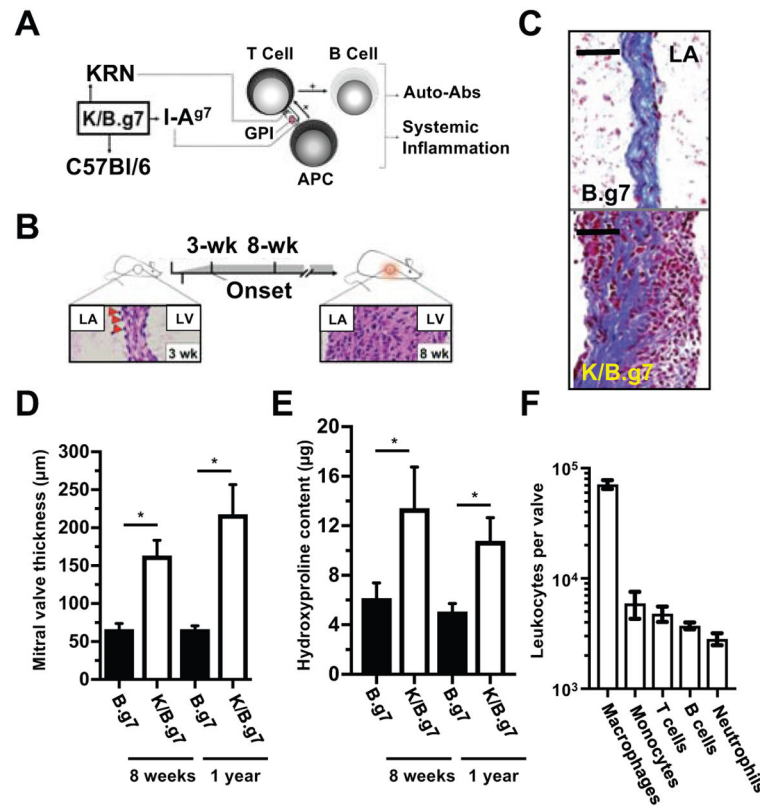


**Figure 1. Fully-penetrant, fibro-inflammatory cardiac valve pathology in K/B.g7 mice**  
**A**, K/B.g7 mice develop systemic inflammation and auto-antibody production following activation of T lymphocytes bearing a transgenic T cell receptor (TCR, termed ‘KRN’) that recognizes a peptide derived from glucose-6-phosphate-isomerase (GPI) presented in the context of the I-Ag7 major histocompatibility complex-II (MHC-II) expressed on professional antigen-presenting cells (APCs). **B**, K/B.g7 mice develop fully-penetrant cardiac valve inflammation and fibrosis beginning at 3 weeks of age (evident histologically by the appearance of adherent inflammatory cells at the mitral valve (MV)-atrial interface, bottom left image, red arrowheads) and by 8 weeks of age, the MV becomes dramatically thickened and diffusely inflamed (bottom right image). **C**, Masson’s trichrome staining of coronal sections at 8 weeks of age shows that in non-inflamed B.g7 control mice that lack expression of the transgenic KRN TCR the MVs are homogeneous, thin, collagen-rich, and sparsely-cellular (top), whereas age-matched K/B.g7 MVs (bottom) demonstrate dramatic structural alterations resulting interstitial collagen deposition and diffuse infiltration of mononuclear inflammatory cells. **D**, The inflamed K/B.g7 MVs are thickened approximately 2.5-fold relative to the non-inflamed B.g7 control mice at both 8 weeks and 1 year of age (median MV thickness, 8-weeks: 68.1 µm [n=4] and 180.3 µm [n=4]; median MV thickness, 1-year: 66.4 µm [n=3] and 217.7 µm [n=3], in B.g7 and K/B.g7 mice, respectively) **E**, Quantifiably-elevated hydroxyproline (HYP) content (a measure of collagen) is present in K/B.g7 MVs, both at 8-weeks and also 1-year, relative to non-inflamed control mice (median MV HYP content, 8-weeks: 7.16 µg [n=5] and 10.3 µg [n=3]; median MV HYP content, 1-year: 4.6 µg [n=4] and 10.2 µg [n=4]; B.g7 and K/B.g7 mice, respectively). **F**, Flow

cytometry of collagenase-2-DNAse-I-digested MVs from K/B.g7 mice demonstrates a leukocytic infiltrate (CD45.2<sup>+</sup> fraction) dominated by mononuclear phagocytes (MNPs, e.g. macrophages and monocytes) while T and B lymphocytes and neutrophils are present less frequently (n=5). 'LV' and 'LA' denotes the left ventricle and left atrium, respectively. Scale bars in **C** are equal to 50 microns. Asterisks (\*) in **D** and **E** indicate statistical significance at p<0.05.

Author Manuscript

Author Manuscript

Author Manuscript

Author Manuscript

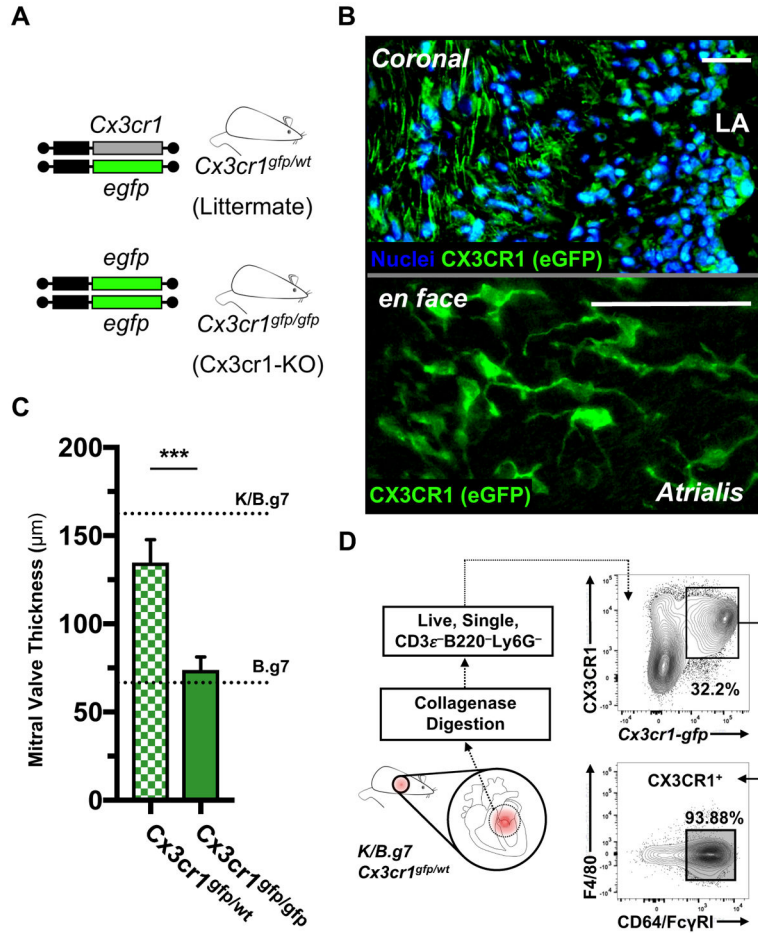


**Figure 2. K/B.g7 cardiac valve inflammation and fibrosis requires CX3CR1**

**A**, *Cx3cr1-gfp* mice contain an eGFP reporter construct in the endogenous *Cx3cr1* locus; mice homozygous for the eGFP allele are *Cx3cr1*-null (*Cx3cr1*-KO) whereas heterozygous mice retain *Cx3cr1* expression. **B**, Top: *Cx3cr1-eGFP<sup>+</sup>* cells are seen throughout the MV interstitium of K/B.g7:*Cx3cr1<sup>gfp/wt</sup>* mice (coronal sections, nuclear counter-staining with Hoechst 33342); bottom: *Cx3cr1-eGFP<sup>+</sup>* cells in inflamed K/B.g7 MVs exhibit a characteristic phagocyte morphology (whole-mount MVs from K/B.g7:*Cx3cr1<sup>gfp/wt</sup>* mice, processed using tissue clearing methods and imaged *en face*). **C**, MV thickness measurements from *Cx3cr1*-KO animals (*Cx3cr1<sup>gfp/gfp</sup>*) relative *Cx3cr1*-replete controls (*Cx3cr1<sup>gfp/wt</sup>*) (median MV thickness at 8 weeks: 132.9 µm [n=4] and 69.1 µm [n=10], *Cx3cr1<sup>gfp/wt</sup>* and *Cx3cr1<sup>gfp/gfp</sup>*, respectively); reference thicknesses for MVs from K/B.g7 and B.g7 control mice are provided. **D**, Flow cytometry on collagenase-2-DNAse-I-digested MVs from K/B.g7:*Cx3cr1<sup>gfp/wt</sup>* mice demonstrating GFP<sup>+</sup> MNPs (CD45.2<sup>+</sup>CD3<sup>ε</sup><sup>-</sup>B220/CD45R<sup>-</sup>Ly6G<sup>-</sup>CX3CR1<sup>+</sup>) uniformly display a phenotype consistent with macrophages (CD64/FcγRI<sup>+</sup>), therein. Scale bars in **B** are equal to 50 microns. Asterisks (\*\*\*) in **C** indicate statistically significant differences at p<0.005.

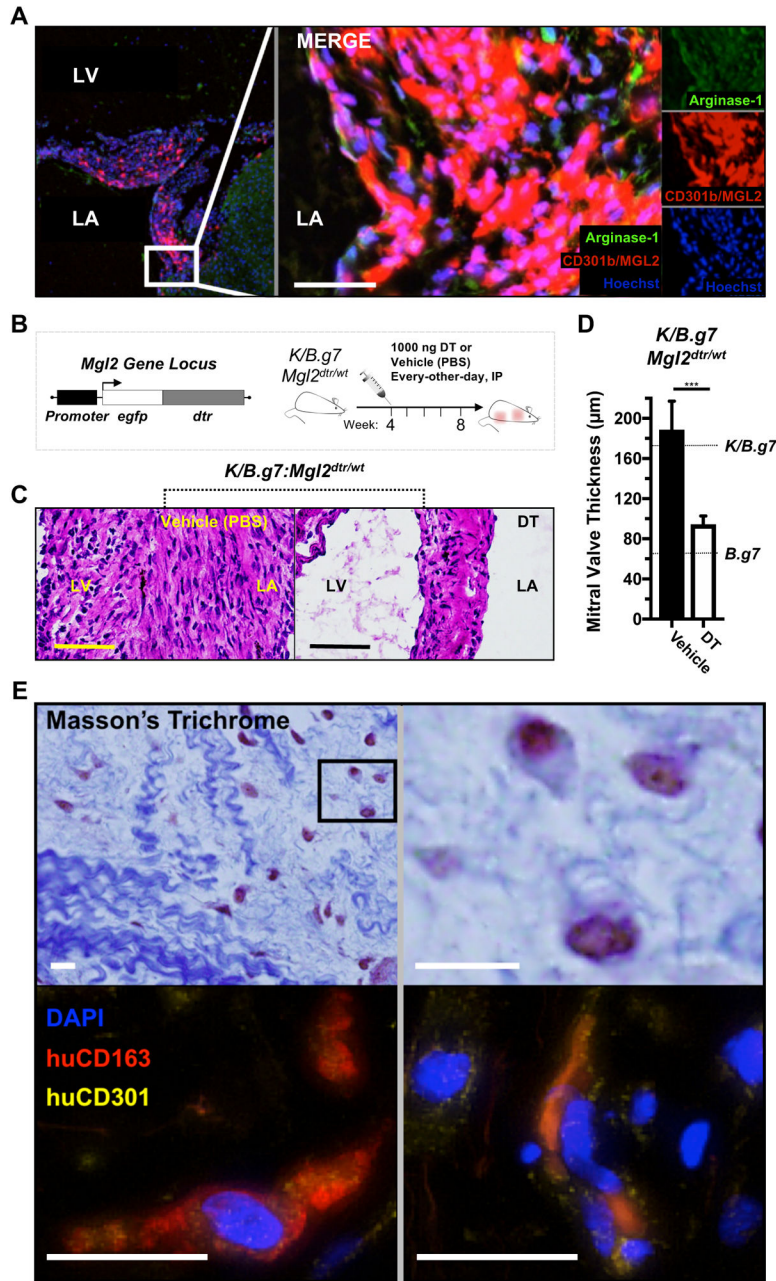


**Figure 3. CD301b/MGL2-expressing MNPs are necessary for K/B.g7 MV inflammation and fibrosis and have correlates in human inflammatory MV disease**

**A**, Immunofluorescent (IF) imaging of K/B.g7 MVs in coronal sections showing diffuse interstitial infiltration of tissue-reparative CD301b/MGL2<sup>+</sup>Arg-1<sup>+</sup> inflammatory cells. **B**, Top left: mice expressing a diphtheria toxin (DT) receptor (DTR)-eGFP construct under control of the *Mgl2* gene (*Mgl2-DTR*) were generated on the K/B.g7 background (K/B.g7:*Mgl2*<sup>dtr/wt</sup>); top right: *Mgl2*-expressing cell ablation was initiated at 4-weeks of age with intraperitoneal (IP) injections of 1 µg DT (or vehicle/PBS), repeated every-other-day for a total of 4-weeks (timeline at bottom). **C**, Depletion of CD301b/MGL2-expressing cells results in qualitatively reduced valve inflammation and fibrosis relative to vehicle-treated

control animals, as demonstrated by H&E staining. **D**, MVs are significantly less fibrotic and inflamed in the setting of CD301b/MGL2-expressing cell depletion (median MV thicknesses at 8 weeks: 148.0  $\mu\text{m}$  [n=7] and 83.4  $\mu\text{m}$  [n=5], vehicle- and DT-treated K/B.g7:*Mgl2<sup>dtr/wt</sup>* mice, respectively, \*\*\*p<0.005); the dashed lines represent reference thicknesses for MVs from K/B.g7 and B.g7 controls. **E**, Top: Masson's trichrome staining of a pathology sample taken from a young adult patient with mitral regurgitation (MR) secondary to rheumatic heart disease (RHD) displaying structural degeneration and leukocytic infiltration into the valve interstitium (top); bottom: IF staining of the same sample reveals co-expression of human CD301 (CLEC10) and the pan-macrophage marker CD163 within the inflamed MV interstitium. Scale bars in all images are equal to 50 microns.

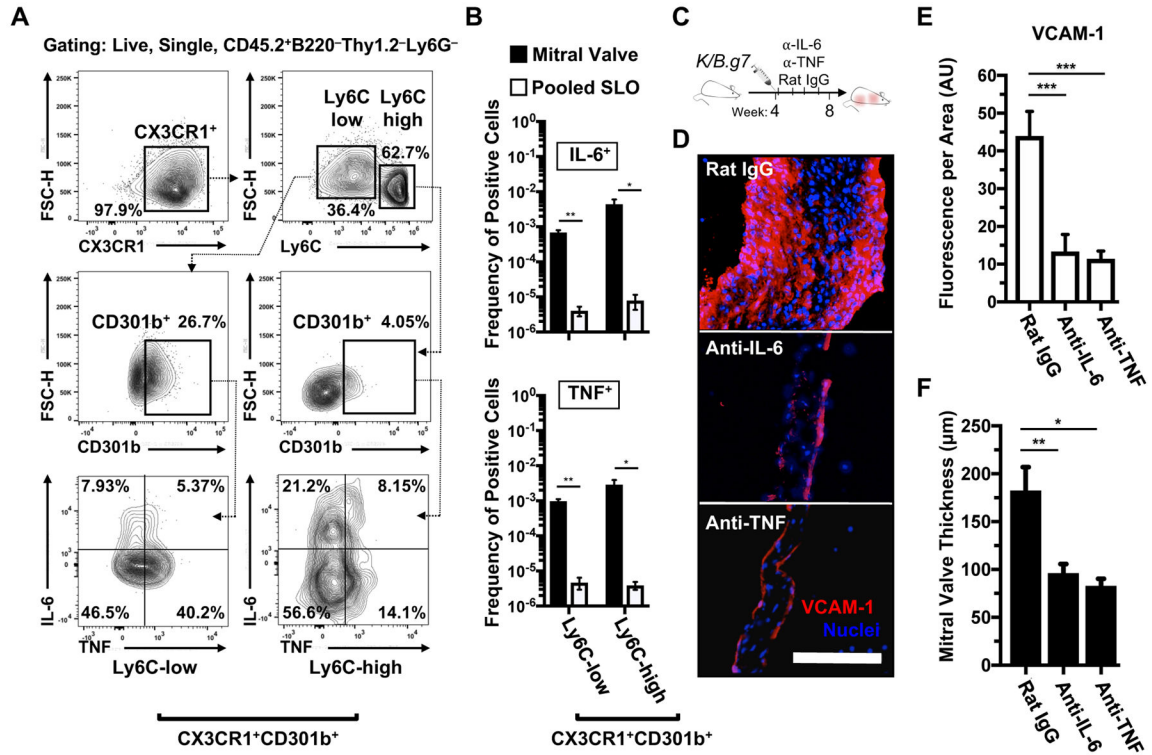


**Figure 4. TNF- and IL-6-producing CX3CR1+CD301b/MGL2+ MNPs are enriched in inflamed cardiac valves and blockade of either cytokine prevents valve inflammation and fibrosis**

**A**, Gating strategy for identifying and discretizing CD301b/MGL2-expressing MNPs (Live, CD45.2<sup>+</sup>Thy1.2<sup>-</sup>B220<sup>-</sup>Ly6G<sup>-</sup>CX3CR1<sup>+</sup>) based on Ly6C expression to assess their TNF and IL-6 production capacity (positive gating for CD301b/MGL2, TNF and IL-6 expression was generated from each respective fluorescence-minus-one [FMO] control). **B**, Quantification of TNF- and IL-6-producing CX3CR1<sup>+</sup>CD301b/MGL2<sup>+</sup> MNPs in inflamed K/B.g7 MVs relative to the systemic circulation (pooled secondary lymphoid organs [SLO]: axillary, brachial, cervical, inguinal, popliteal, para-aortic, mesenteric lymph nodes and spleens) (\*p<0.05, \*\*p<0.01, n=3). **C**, Timeline for TNF and IL-6 blockade studies: twice-weekly, IP injections of 200 µg of either anti-TNF or anti-IL-6 (or rat IgG as a control) were given from weeks 4 to 8. **D**, IF staining for vascular cell adhesion molecule-1 (VCAM-1) following TNF or IL-6 blockade, relative to rat IgG. **E**, Quantification of VCAM-1 fluorescence, normalized to MV area, following TNF or IL-6 blockade, relative to isotype control-treated K/B.g7 animals (median fluorescence/area [arbitrary units]: 44.86 [n=4], 16.22 [n=4], 11.2 [n=4], rat IgG-, and anti-IL-6, anti-TNF, respectively, \*\*\*p<0.005). **F**, Quantification of MVs fibrotic thickening in the setting of TNF or IL-6 blockade, relative to isotype control-treated animals (median MV thicknesses at 8 weeks: 162.5 µm [n=6], 98.3 µm [n=5], 88.05 µm [n=4] rat IgG-, and anti-IL-6, anti-TNF respectively, \*p<0.05, \*\*p<0.01). Scale bar in **D** equals 50 microns and applies to all images. Statistical differences in **E** and **F** were assigned using one-way analysis of variance (ANOVA) with post-hoc Tukey’s test for multiple comparisons.

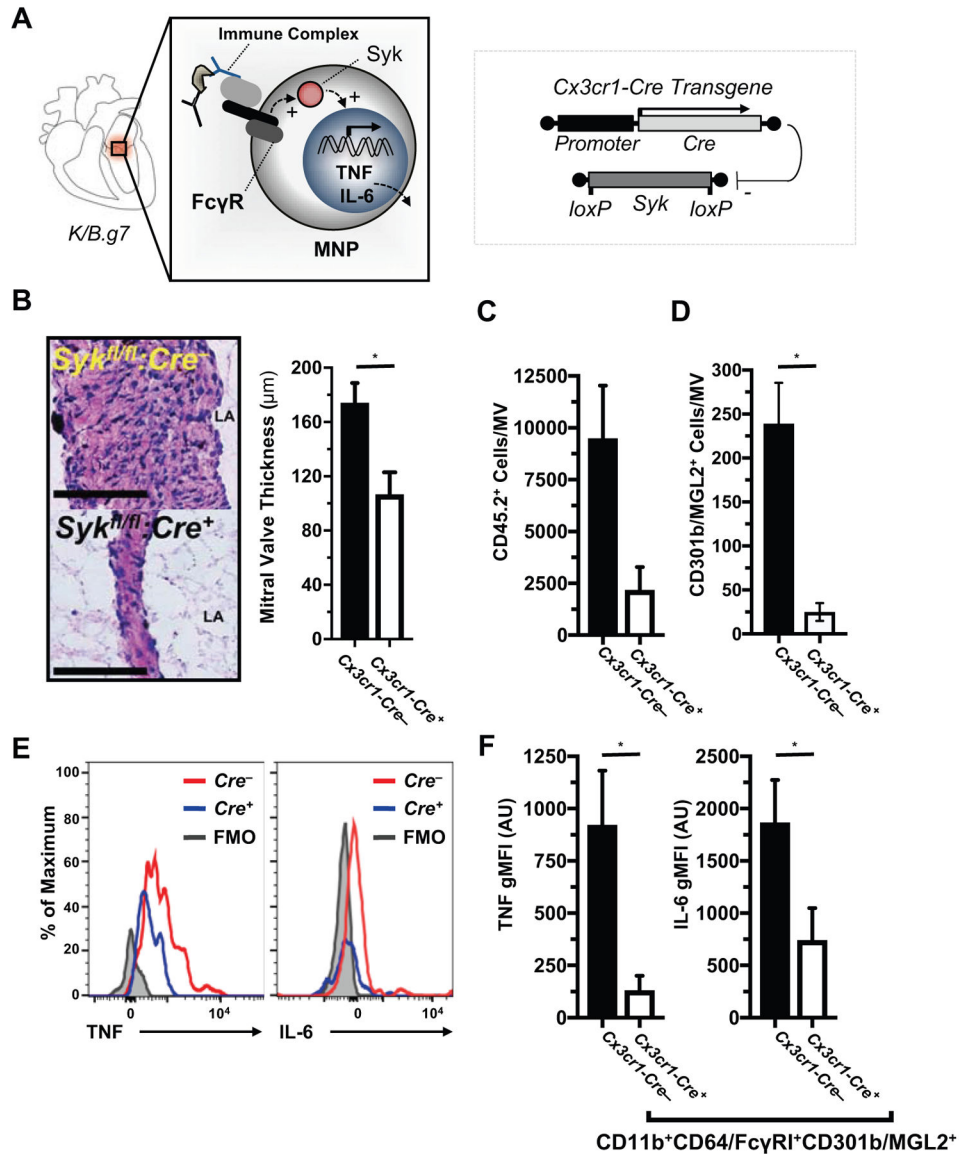


**Figure 5. Fc $\gamma$ R-Syk signaling in CX3CR1<sup>+</sup>CD310b/MGL2<sup>+</sup> phagocytes drives TNF and IL-6 production**

**A**, left: a diagram of Syk-dependent Fc $\gamma$ R signaling as a hypothesized mechanism for auto-antibody-mediated TNF and IL-6 production from valve-infiltrating MNPs; right: conditional deletion of MNP-*Syk* was accomplished using *Cx3cr1-Cre*. **B**, Histological assessment and quantification of MV fibrotic thickening in K/B.g7 mice with MNPs conditionally lacking *Syk* ( $Cx3cr1-Cre^+; Syk^{fl/fl}$ ) versus their *Syk*-replete littermates ( $Cx3cr1-Cre^-; Syk^{fl/fl}$ , median MV thicknesses at 8 weeks: 183.3  $\mu\text{m}$  [n=11] and 83.4  $\mu\text{m}$  [n=11],  $Cx3cr1-Cre^-; Syk^{fl/fl}$  and  $Cx3cr1-Cre^+; Syk^{fl/fl}$ , respectively; scale bars are equal to 50 microns). Quantification of total leukocytes (**C**, CD45.2<sup>+</sup> cells) and CD301b/MGL2<sup>+</sup> MNPs (**D**, CD45.2<sup>+</sup>CD3e<sup>-</sup>B220/CD45R<sup>-</sup>Ly6G<sup>-</sup>CD11b<sup>+</sup>CD64/Fc $\gamma$ RI<sup>+</sup>) in MVs from MNP-*Syk*-replete ( $Cre^-$ ) versus MNP-*Syk*-deleting mice ( $Cre^+$ ) (n=7  $Cx3cr1-Cre^-; Syk^{fl/fl}$ , n=5  $Cx3cr1-Cre^+; Syk^{fl/fl}$ ). **F**, Quantification of intracellular TNF (left) and IL-6 (right)



production (geometric mean fluorescence intensity [gMFI]) from MV cells in Syk-deleting and non-deleting mice. Asterisks (\*) indicate statistical significance at  $p < 0.05$ . 'AU' indicates arbitrary units.

Author Manuscript

Author Manuscript

Author Manuscript

Author Manuscript

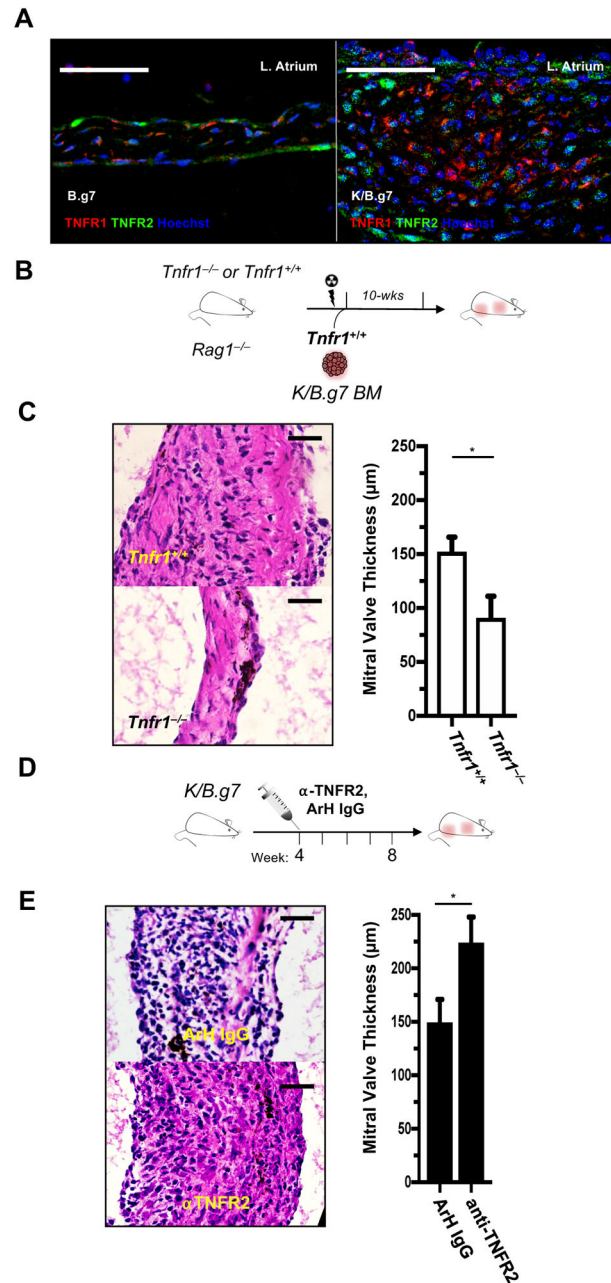


**Figure 6. TNFR1 promotes MV disease while TNFR2 restrains it**

**A**, Immunofluorescence (IF) of TNFR1 and TNFR2 in an 8-week K/B.g7 MV (right) and a non-inflamed, B.g7 control (left). **B**, Experimental design used to generate bone marrow (BM) chimeric mice. **C**, Left: Qualitative assessment of MV inflammation in BM recipient mice; right: quantification of MV thicknesses from *Tnfr1*<sup>+/+</sup> and *Tnfr1*<sup>-/-</sup> recipients (median 8-week MV thicknesses: 154.5 μm [n=8], 75.8 μm [n=8], *Tnfr1*<sup>+/+</sup> and *Tnfr1*<sup>-/-</sup>, respectively, \*p<0.05). **D**, Experimental design for blockade of TNFR2 from weeks 4–8. **E**, left: H&E staining of MV sections from anti-TNFR2 IgG-treated K/B.g7 mice compared to isotype (Armenian hamster [ArH] IgG) control-treated animals; right: MV thickness

quantification in the setting of TNFR2 blockade (median 8-week MV thicknesses: 151.0  $\mu\text{m}$  [n=7], 228.8  $\mu\text{m}$  [n=4], ArH IgG, anti-TNFR2, respectively, \*p<0.05). Scale bars in **A**, **C**, and **E** equal 50 microns.

Author Manuscript

Author Manuscript

Author Manuscript

Author Manuscript

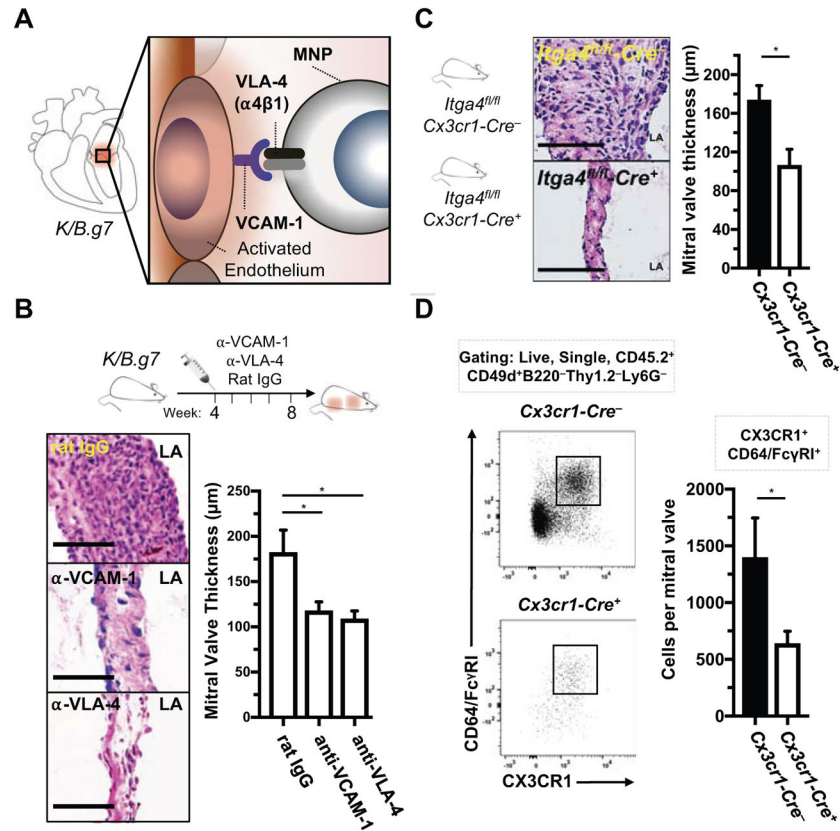


**Figure 7. Accumulation of cardiac valve-infiltrating CX3CR1<sup>+</sup> mononuclear phagocytes is dependent on VCAM-1:VLA-4 interactions**

**A**, Diagram of a hypothesized mechanism for TNF- and IL-6-mediated MNP accumulation in K/B.g7 MVs via VCAM-1:VLA-4 interactions. **B**, Experimental design for monoclonal antibody blockade of either VCAM-1 or VLA-4 from weeks 4–8 (top); histological assessment of MV inflammation and fibrosis each case (bottom left); quantification of MV fibrotic thickening for each case (bottom right) (median 8-week MV thicknesses: 162.5 µm [n=6], 109.9 µm [n=8], 110.5 µm [n=6] rat IgG, anti-VCAM-1, anti-VLA-4 respectively, \*p<0.05). **C**, Conditional deletion of *Itga4* in MNPs (MNP-*Itga4*) was accomplished using *Cx3cr1-Cre<sup>+</sup>:Itga4<sup>fl/fl</sup>* mice on the K/B.g7 background and compared to *Cre*-negative littermates (diagrammed at left); conditional deletion of MNP-*Itga4* qualitatively reduces MV inflammation and fibrosis that is evident histologically (middle); quantification of MV thicknesses in the setting of conditional MNP-*Itga4* deletion, relative to MNP-*Itga4*-replete animals (median 8-week MV thicknesses: 144.5 µm [n=14], 104.8 µm [n=8], *Cx3cr1-Cre<sup>-</sup>:Itga4<sup>fl/fl</sup>*, *Cx3cr1-Cre<sup>+</sup>:Itga4<sup>fl/fl</sup>*, respectively). **D**, Flow cytometry gating strategy for analysis of K/B.g7 MVs in the setting of conditional MNP-*Itga4* deletion; quantification of total ITGA4/CD49d (α4 integrin)-expressing leukocytes (CD.45.2<sup>+</sup> cells) and macrophages (CX3CR1<sup>+</sup>CD64/FcγRI<sup>+</sup>) in each genetic condition (bottom right) (n=7, *Cre<sup>-</sup>*, n=9 *Cre<sup>+</sup>*, \*p<0.05). Scale bars are equal to 50 microns in all images. Statistical differences in **B** were assigned using one-way analysis of variance (ANOVA) with post-hoc Tukey's test for multiple comparisons.

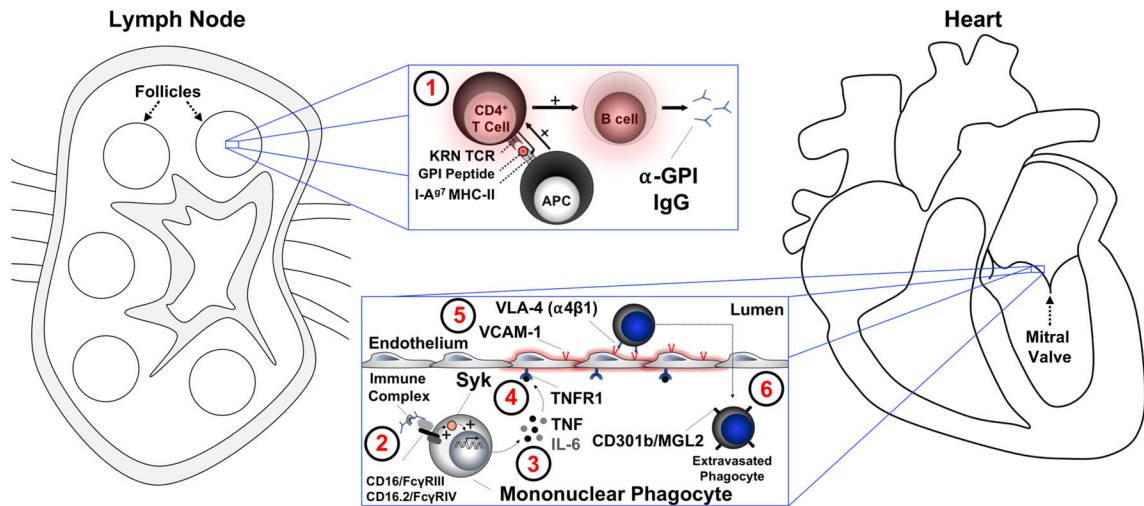


**Figure 8. A summary working model for the initiation of cardiac valve inflammation and fibrosis in K/B.g7 mice**

Anti-glucose-6-phosphate isomerase ( $\alpha$ -GPI) IgG auto-antibodies produced systemically in the secondary lymphoid tissue (spleen and lymph nodes) (1) activate valve-infiltrating mononuclear phagocytes (MNPs) in a spleen tyrosine kinase (Syk)-dependent process (2) resulting in local production of TNF and IL-6 from  $CX3CR1^+CD301b/MGL2^+$  MNPs. Tumor necrosis factor receptor-1 (TNFR1)-mediated activation of the valve stroma (3) promotes vascular cell adhesion molecule-1 (VCAM-1) upregulation (4) and subsequent recruitment of additional circulating  $CX3CR1^+$  MNPs via very-late antigen-4 (VLA-4,  $\alpha4\beta1$  integrin) in a feed-forward process (5). Interstitial MNPs assume a tissue-reparative phenotype characterized by expression of CD301b/MGL2, resistin-like molecule-alpha (RELM- $\alpha$ ), and arginase-1 (Arg-1) (6). Explanation of terms: KRN TCR: transgenic T cell receptor; I-A<sup>g7</sup> MHC-II: major histocompatibility complex-II from the non-obese diabetic (NOD) mouse strain; APC: antigen presenting cell (e.g. dendritic cells); MGL2: macrophage galactose N-acetyl-galactosamine specific lectin 2.